Conf-9107115--73

X-ray Diffraction Study of GaSb/AlSb Strained-Layer-Superlattices Grown on Miscut (100) Substrates*

A.T. Macrander
Advanced Photon Source
Argonne National Laboratory
9700 South Cass Avenue
Argonne, IL 60439

G.P. Schwartz, G.J. Guiltieri, and G. Gilmer
AT&T Bell Laboratories
Murray Hill, NJ

ANL/CP--72290

DE92 009734

July, 1991

*This work supported by the U.S. Department of Energy, BES-Materials Sciences, under contract no. W-31-109-ENG-38

X-ray diffraction study of GaSb/AlSb strained-layer-superlattices grown on miscut (100) substrates

A.T. Macrander *

Argonne National Laboratories, Advanced Photon Source, Argonne , IL 60439

G.P. Schwartz, G.J. Gualtieri, and G. Gilmer

AT&T Bell Laboratories, Murray Hill, NJ 07974

ABSTRACT

A series of superlattices were grown by molecular beam epitaxy on (100) GaSb substrates which had been miscut by 2,3, and 4 degrees toward the <011> direction. These superlattices were then studied by scanning all possible {444} or {511} (asymmetric) reflections with high resolution multiple-crystal x-ray diffractometry. In addition, the (400) (quasi-symmetric) reflection was scanned . From peak splittings we extracted mismatch and tilt parameters for the epitaxial unit cell. We compared our results for the non-tetragonal component of the distortion to calculations based on the coherent strain model of Hornstra and Bartels (J. Cryst. Growth 44 , 513 (1978)). We find that this model which was developed for epitaxial growth on a general (hkl) plane also describes our results for growth on vicinal (100) planes. The resolution of our data is sufficient to establish that the distortion was not purely tetragonal. A monoclinic unit cell symmetry adequately descibes our results.

Introduction

We have examined the fundamental elastic distortions which occur in coherently strained epitaxial films of lattice-mismatched material grown on miscut (100) substrates. We find that there is a non-tetragonal component of the distortion which involves a tilt and that this tilt is small for small angles of miscut. Because tilts are small for the range of miscuts commonly used for MBE substrates, a high resolution x-ray measurement is needed.

* data obtained while at AT&T Bell Laboratories, Murray Hill, NJ

Coherent epitaxy on vicinal (100) substrates can be viewed in the more general context of growth on arbitrary (hkl) planes. We compare our results to calculated predictions based on the elastic description of Hornstra and Bartels[1]. The original intent of the mathematical framework developed by Hornstra and Bartels was to describe strains in epitaxial layers grown directly on any (hkl) plane (e.g., (100), (111), (311)). We have successfully applied this same formalism to our results by considering very high index surfaces (e.g, (27,1,1) for 3 deg miscut).

It is important to distinguish coherently strained films from films which relax via the formation of misfit dislocations because distortions associated with the introduction of misfit dislocations can potentially mask displacements related to coherent growth[2]. To sort out the different origins of tilts we made measurements on two sets of superlattices. For the first set no misfit dislocations were present. This was corroborated by the mismatch measurements, since no lateral (i.e., along the <010> direction) mismatch was found. For the second set misfit dislocations were present, and lateral mismatch was measured. We find that the misfit dislocations did not alter the measured tilts. This result implies that for the range of miscut angles which we investigated, tilts due to misfit dislocations did not add up in a coherent fashion.

Nagai[3] has speculated that the strain at a stepped interface produces tilts as shown in Fig. 1. We were interested in determining the actual strain due to a stepped interface.

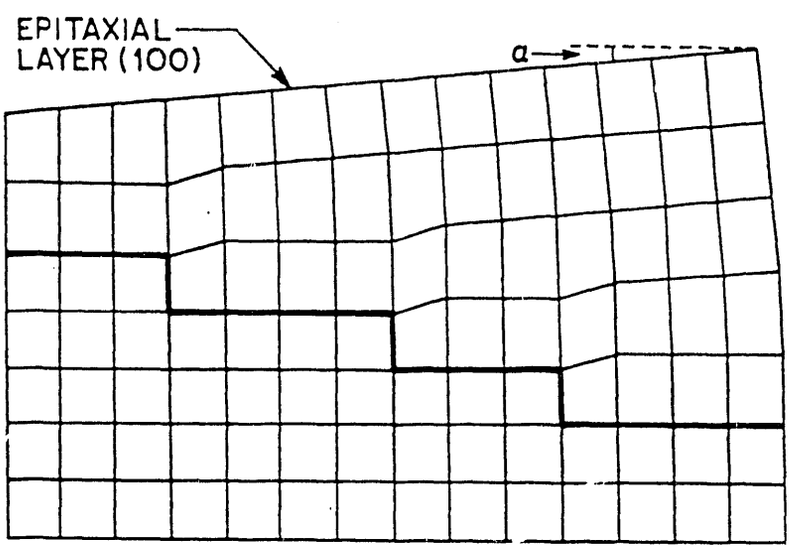

Fig.1. Speculation of strain at stepped interface (ref. 3).

We chose the GaSb/AlSb superlattice system for this study because of the large range of mismatch , 0.65%, available and because both coherent and incoherent superlattices with convenient and useful overall thicknesses could be grown controllably and reproducibly by molecular beam epitaxy (MBE). (Single epitaxial layers of AlSb are much harder to handle due to the reactivity of AlSb with room ambients). The measurements which we report here all apply to the average lattice of the superlattice and not to the lattices of either the GaSb or the AlSb layers individually. That is, our results were all obtained from splittings between the zero-order superlattice Bragg peak and the substrate Bragg peak.

Crystal Growth and Diffractometry Details

An undoped GaSb boule was aligned using a Laue backscattering camera, and (100) slices were cut misoriented by 0,2,3 and 4° towards <011>. These wafers were polished with bromine-methanol and cleaned *in vacuo* under an antimony flux in a non-commercial MBE apparatus. Superlattices consisting of 6 periods of 75 Å / 75 Å AlSb / GaSb were grown on each of the miscut substrates at 520 ° C from elemental sources. Both the total superlattice thickness (900 Å) and the 75 Å layer thickness for AlSb are consistent with misfit -free, coherent epitaxy in this system [4]. A second series of samples consisting of 16 periods with the same layer thicknesses was also grown. For this latter case the superlattice is sufficiently thick (2400 Å) that misfit dislocations were anticipated . Table I identifies the properties of each superlattice.

Table I. Superlattice sample description

Sample number	Number of periods	Miscut angle (degrees)
1	6	0
2	6	2
3	6	3
4	6	4
5	16	0
6	16	2
7	16	3
8	16	4

The diffraction data were obtained with a custom high resolution diffractometer provided by Blake Industries and placed on a rotating copper anode source. The monochromator stage of this diffractometer is shown in Fig.2. The first crystal was a Ge crystal miscut by 3.7° from (100). We used the (311) reflection from this crystal. The asymmetry factor in this case is b= – 0.12. We employed mostly the (311)a configuration with the incident beam from the anode entering at a high angle and the beam exiting from the first crystal at a low angle. The effect of this arrangement is to concentrate the radiation in a smaller area on the sample. A second channel-cut Ge crystal followed the first crystal in the x-ray optical path. The channels were (111) faces and we used (333) reflections. The first crystal and the first face of the channel-cut crystal form a (+,+) arrangement, and this provides high resolution. The second reflection of the channel-cut crystal redirected the beam conveniently. The (+,+) arrangement forms a true monochromator and is wavelength-dispersion free for all samples . This is a powerful advantage over a double crystal arrangement which is wavelength-dispersion free only if the Bragg spacings for the first and second crystals are the same. The $CuK\alpha_1$ and $CuK\alpha_2$ lines were well separated in the present arrangement , and we aligned the mononchromator to pass $CuK\alpha_1$. We used a Peltier-cooled lithium-drifted silicon detector to obtain the diffraction data. The dark count rate with this detector was 1 count in 3 minutes .

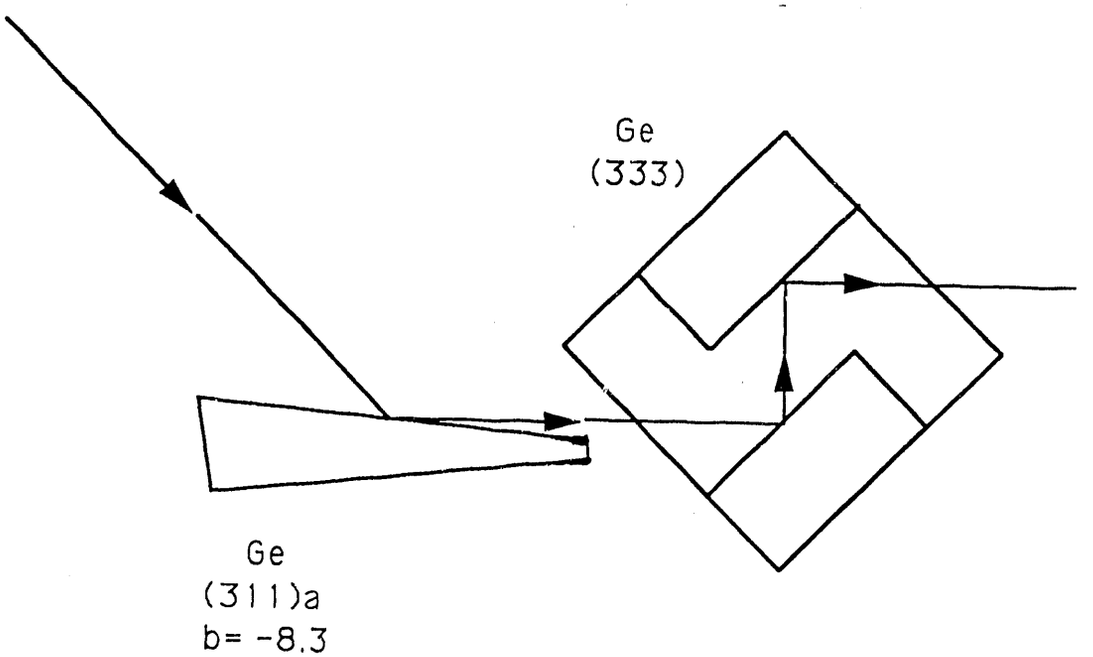

Fig.2. High resolution monochromator stage.

Asymmetric Reflection Method and Data Analyses

Diffraction from the {444} planes was examined for superlattices with 6 and 16 periods offcut by 2 and 3°. The scattering geometries employed on the terraced samples are schematically depicted in Fig.3. The vector $\mathbf{v}_d$ points in the 'downstairs' <011> direction of the terrace. There are two possible {444} reflections with the sample positioned on the diffractometer so that $\mathbf{v}_d$ lies in the diffraction plane. We have indexed the reflection which has its reciprocal lattice vector towards the 'downstairs' side as the (444) reflection and the one on the upstrairs side as the $(4\bar{4}\bar{4})$. Similarly, there are two possible {444} reflections at 90° to the terrace direction. These are $(4\bar{4}4)$ and $(44\bar{4})$. Each of these asymmetric reflections was scanned twice, once with a low incidence angle which we have designated as 'b' scans and once with a high incidence angle which we have designated as 'a' scans.

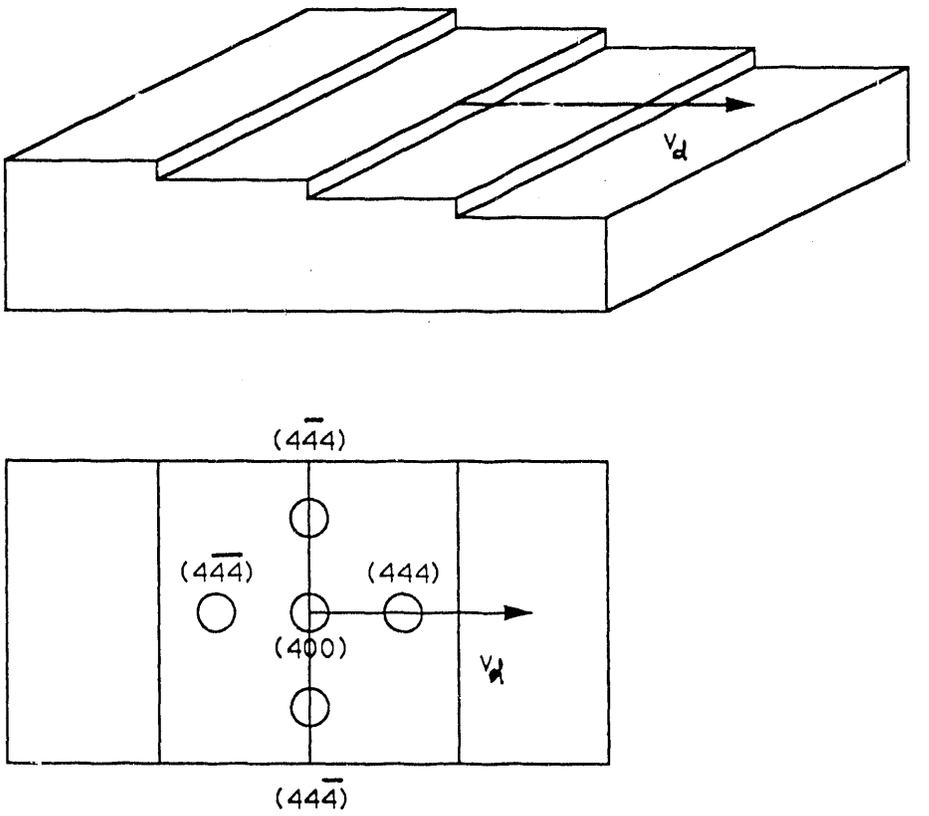

Fig.3. Relationship between terrace direction and reciprocal space.

For coherently strained epitaxy on flat (100) planes (i.e.,zero miscut angle), the epitaxial lattice symmetry is pure tetragonal and the angular difference between the peaks has two sources[5]. The first part is denoted as $\Delta\Theta$ and is due to a difference in Bragg spacing which causes a difference in Bragg angle. The second part results from the relative inclination of equivalent planes and is denoted as $\Delta\Psi$. For analyses of the present data we found that the tetragonal symmetry was lowered since different values of $\Delta\Theta$ and $\Delta\Psi$ were obtained for the (444) reflection than for the $(4\overline{44})$ reflection (i.e., the in-terrace cases). We made our analyses by replacing $\Delta\Theta$ and $\Delta\Psi$ with $(\Delta\Theta+\delta_\theta)$ and $(\Delta\Psi+\delta_\psi)$. The angular separation between peaks for all of the four in-terrace cases are given below:

$$\omega_{(444)a} = (\Delta\Theta+\delta_\theta)+(\Delta\Psi+\delta_\psi) \qquad 1(a)$$

$$\omega_{(444)b} = (\Delta\Theta+\delta_\theta)-(\Delta\Psi+\delta_\psi) \qquad 1(b)$$

$$\omega_{(4\overline{44})a} = (\Delta\Theta-\delta_\theta)+(\Delta\Psi-\delta_\psi) \qquad 1(c)$$

$$\omega_{(4\overline{44})b} = (\Delta\Theta-\delta_\theta)-(\Delta\Psi-\delta_\psi) \qquad 1(d)$$

Plus signs within the parentheses are for the downstairs cases and minus sign are for the upstairs cases. The 'a' cases have a plus sign between the θ and ψ terms and the 'b' cases have minus sign because the samples were rotated by 180° between the two.

A similar analyses was also made for the out-of-terrace cases. The out-of-terrace cases, however, were not expected to exhibit non-tetragonal symmetry, and we expected to find $\delta_\theta = \delta_\psi = 0$. Equations 1(a) through 1(d) constitute four equations and four unknowns.

An example scan is shown in Fig.4. Our angular separations are all referenced to the substrate peak which leads to negative values for the ω's. The data are listed in Table II.

From Table II it is clear that the in-terrace and out-of-terrace cases are qualitatively different. By employing Eqs.1a-d, we obtained the results shown in Table III.

These results clearly show that δ_θ for the in-terrace case is not zero. We consider the δ_θ and δ_ψ values for the out-of terrace cases to be an indicator of our precision. The results listed in Table III would be obtained if the unit cell

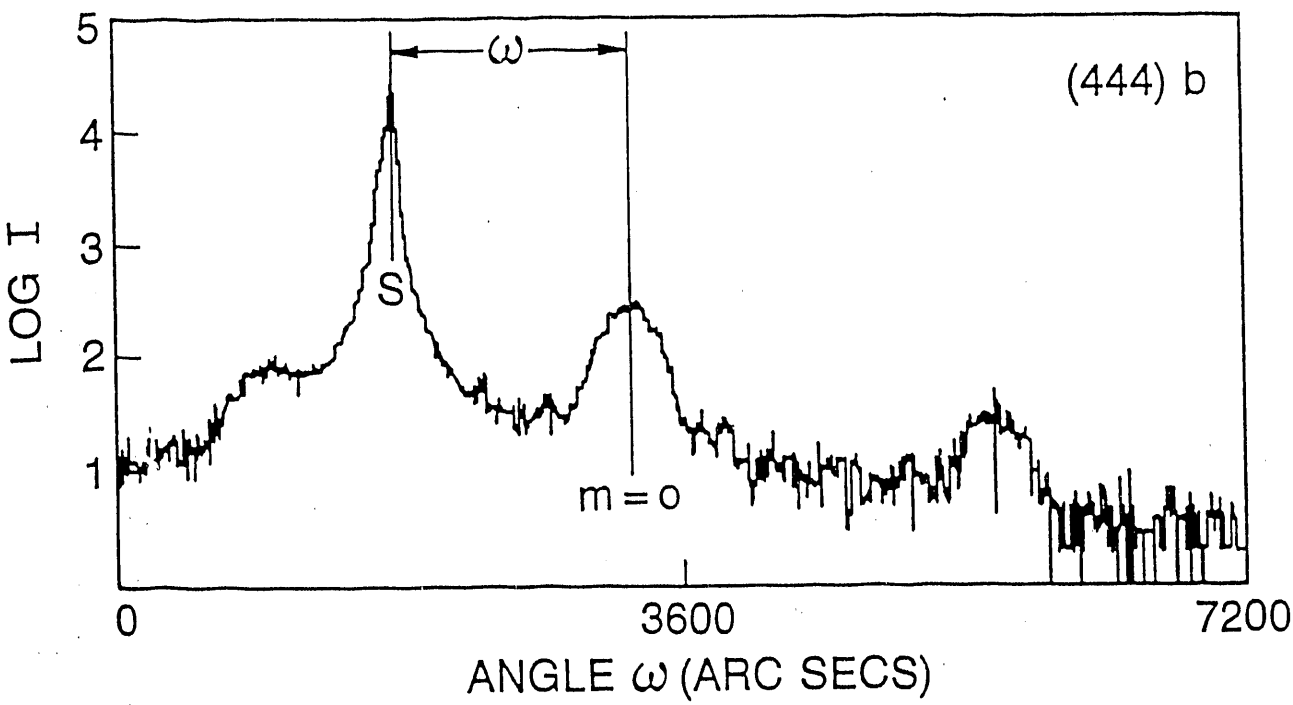

Fig.4. Example data scan.

Table II. Observed {444} or {511} peak separations (in arc sec).

		in-terrace				out-of-terrace			
Sample	miscut	$\omega_{(444)a}$	$\omega_{(444)b}$	$\omega_{(4\bar{4}4)a}$	$\omega_{(4\bar{4}4)b}$	$\omega_{(4\bar{4}\bar{4})a}$	$\omega_{(4\bar{4}\bar{4})b}$	$\omega_{(44\bar{4})a}$	$\omega_{(44\bar{4})b}$
2	2°	-114	-1453	-261	-1553	-192	-1500	-205	-1563
3	3°	-90	-1488	-276	-1584	-162	-1524	-210	-1518
6	2°	-147	-1356	-286	-1476	-203	-1452	-240	-1444
7	3°	(-90)*	-1384	-276	-1464	-293	-1468	-243	-1452
7**	3°	-645	-1408	-808	-1328				

* estimated from shoulder since separate peaks were not resolved

** for {511) reflection

Macrander 7

Table III. Data evaluation results for {444} and {511} scans (in arcsec).

Sample	miscut	in-terrace ΔΘ	in-terrace δ_θ	in-terrace ΔΨ	in-terrace δ_ψ	out-of-terrace ΔΘ	out-of-terrace δ_θ	out-of-terrace ΔΨ	out-of-terrace δ_ψ
2	2°	-845	+62	+658	+12	-865	+19	+667	-13
3	3°	-860	+70	+676	+23	-854	+11	+668	+14
6	2°	-816	+65	+600	+5	-835	+7	+613	+11
7	3°					-864	-17	+596	-9
7*	3°	-1047	+21	+321	+61				

* for {511} reflections.

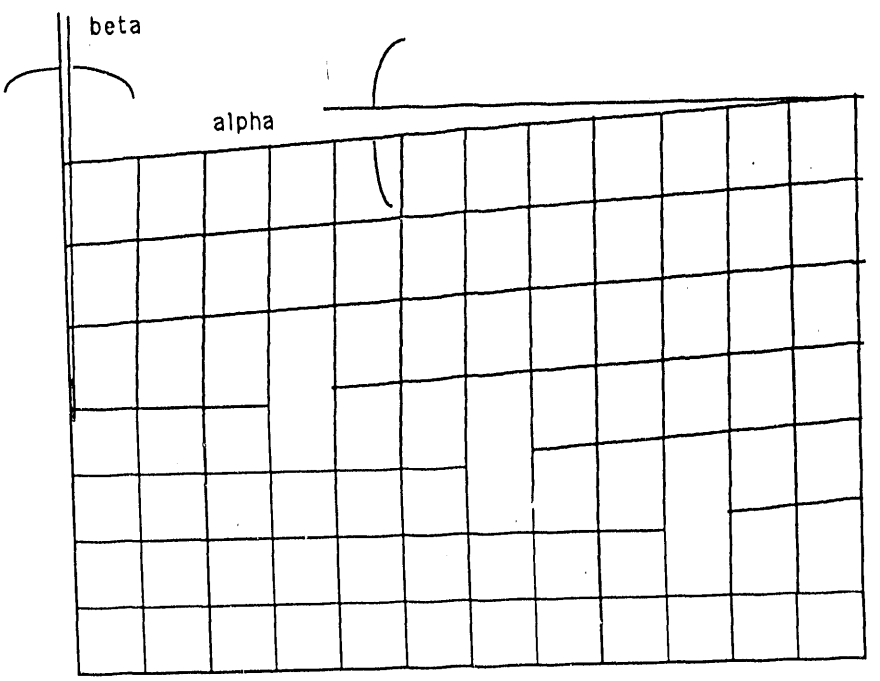

Fig.5. Elastic strain at stepped interface.

symmetry in our case was not triclinic but rather was monoclinic. If the terracing direction is not directly along <011> then a triclinic symmetry can occur[6].

Coherent Strain Model

The strain tensor of the deformed film can be calculated according to the formalism developed by Hornsta and Bartels[1]. From the tensor, calculated values for δ_θ and δ_Ψ can be obtained. In brief, Hornstra and Bartels proceed by first applying a hydrostatic strain to the film until it matches the substrate coherently. The film is then conceptually fitted to the substrate and the stresses applied to the surface are released. By applying the condition that the three Cartesian components of the stress at the surface must be zero, we can obtain the elements of the strain tensor and thus all the strains. For coherent growth on {100}, {110}, and {111} planes the strain tensor is diagonal, and there are no shear strains. For growths on these planes only tetragonal distortion occurs. However, a shear strain also occurs for surfaces of lower symmetry, and for these surfaces the distortion is not simply tetragonal. To compare with our results, diffraction parameters were calculated for {444} reflections on the following growth surfaces: (100), (81,2,2), (27,1,1), and (81,4,4). These growth planes are tipped toward the [011] direction and exhibit miscut angles equal to 0.000, 2.000,2.998, and 3.995 degrees, respectively. The net state of strain is illustrated in Fig.5. For each growth surface $(\Delta d/d)_m$ and $(\Delta\Psi)_m$ were evaluated where $\vec{m}$ refers to one of the <444> directions. In terms of the Hornstra and Bartels formalism these are given by

$$\left[\frac{\Delta d}{d}\right]_m \equiv \frac{d_{film}^{strained} - d_{substrate}^{relaxed}}{d_{film}^{relaxed}} = (\vec{m}\cdot\vec{a})(\vec{m}\cdot\vec{l}) \qquad (2)$$

$$(\Delta\Psi)_m \equiv \Psi_{film}^{strained} - \Psi_{substrate}^{relaxed} = (\vec{m}\cdot\vec{a})\left[1-(\vec{m}\cdot\vec{l})^2\right]^{1/2} \qquad (3)$$

Here $\vec{l}$ is a vector normal to the interface plane, and $\vec{a}$ is the solution of the Hornstra and Bartels formalism for the direction in which all the atoms move when the surface stresses are removed. Calculated values for $(\Delta\Theta)_m$ were obtained from $(\Delta d/d)_m$ values from Bragg's law,

$$(\Delta\Theta)_m = \Delta\Theta \pm \delta_\theta = -\tan\Theta_B(\Delta d/d)_m$$

The results of this calculation are given in Table IV.

Table IV. Calculated {444} non-tetragonal distortion parameters (in arc sec) for GaSb/AlSb superlattices with equal GaSb and AlSb layer thicknesses.

	[1,0,0] 0.000°	[81,2,2] 2.000 °	[27,1,1] 2.988°	[84,4,4] 3.995°
δ_θ	0.0	+42.9	+64.4	+86.0
δ_ψ	0.0	+12.7	+19.0	+25.2

The calculated results in Table IV agree well with those extracted from the data and listed in Table III , and we conclude that Fig.3 illustrates the unit cell symmetry of all our samples.

Lattice Mismatches

The values of $\Delta\Theta$ and $\Delta\Psi$ which we have obtained from the data also allow us to calculate the [100] , [010], and [001] mismatches. This is possible because these quantities are due to the pure tetragonal part of the distortion, and we can apply the known formulas which apply to tetragonal distortion. An examination of Table III shows that the in-terrace and out-of-terrace values for $\Delta\Theta$ and $\Delta\Psi$ are not significantly different which implies that the [010] and [001] mismatches are the same. We have averaged the in-terrace and out-of-terrace values and then used the following formulas for the mismatches[5]:

$$(\Delta a/a)_\perp \equiv (\Delta a/a)_{(100)} = \left[\frac{\sin\Theta_B^s}{\sin(\Theta_B^s+\Delta\Theta)}\frac{\cos\Psi_s}{\cos(\Psi_s+\Delta\Psi)}-1\right], \quad (4)$$

$$(\Delta a/a)_{\parallel} \equiv (\Delta a/a)_{(010),(001)} = \left[\frac{\sin\Theta_B^s}{\sin(\Theta_B^s+\Delta\Theta)}\frac{\sin\Psi_s}{\sin(\Psi_s+\Delta\Psi)}-1\right]. \quad (5)$$

Here Θ_B^s is the Bragg angle of the substrate (61.105° for {444} and 41.044° for {511}), and Ψ_s is the angle between the substrate Bragg planes and the (100) plane (54.736° for {444} and 15.793°} for {511}). Mismatch results are listed in Table VI.

Clearly samples 6 and 7 which have 16 period superlattices are quantitatively different than samples 2 and 3 which have 6 period superlattices. We conclude that the 16 period superlattices were not coherent with the substrate (i.e., they contained misfit dislocations at the substrate/superlattice interface).

Table VI. Tetragonal Mismatches (in per cent) .

Sample	Miscut	$(\Delta a / a)_{\perp}$	$(\Delta a / a)_{\parallel}$
2	2°	0.688	0.004
3	3°	0.695	0.001
6	2°	0.641	0.015
7	3°	0.638	0.033

Lattice Tilts

We have also computed lattice tilts from our measurements. The Hornstra and Bartels[1] formalism predicts that the tilt denoted as α in Fig.5 should be significant in our case[7]. The other tilt shown in Fig.5 which is denoted as β is predicted to be an order of magnitude smaller. We have ignored β in our analyses and thus refer to the distortion as monoclinic and not triclinic. α tilts have been computed from δ_θ and δ_ψ values using the following relationships which we have derived:

$$\alpha = 1.171\delta_\theta^{(444)} \quad , \quad (6)$$

$$\alpha = 4.386\delta_\theta^{(511)} \quad , \quad (7)$$

$$\alpha = 3.00\delta_\psi^{(444)} \quad , \quad (8)$$

$$\alpha = 1.04\delta_\psi^{(511)} \quad . \quad (9)$$

Small angle approximations have been made in the derivation of Eqs.6-9. The results are listed in Table VII and are shown in Fig.6.

Table VII. Lattice tilts (in arc sec) .

sample	miscut	$\alpha(\delta_\theta)$	$\alpha(\delta_\psi)$	$<\alpha>^*$	$\alpha_{(400)}$
1	0				4
2	2	67	51	59	62
3	3	82	69	76	75
4	4				101
6	2	76	15	46	51
7	3	92	63	78	86
8	4				104

* $(\alpha(\delta_\theta) + \alpha(\delta_\psi)) / 2$

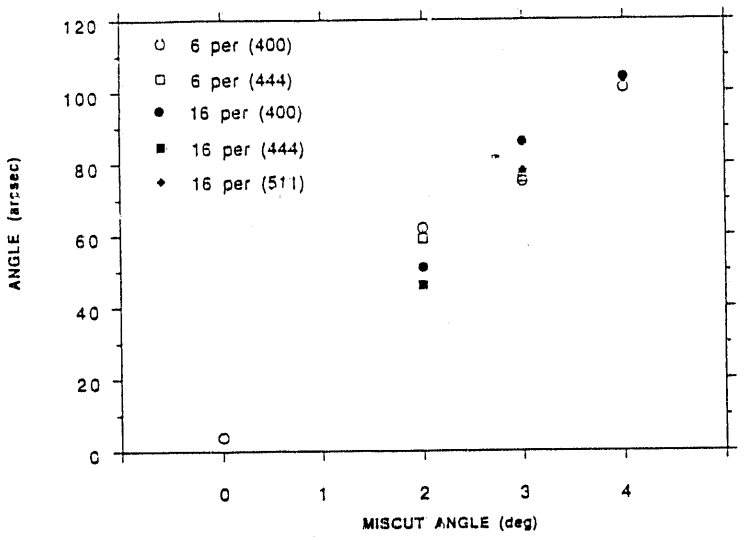

Fig.6. Measured lattice tilts (α).

Also listed in Table VII and plotted in Fig.6 are tilts obtained directly from (400) rocking curves.[5] These results clearly show a systematic increase in tilt with increasing miscut angle, and they do not reveal a significant difference between the 6 period and 16 period samples. We conclude that tilt contributions due to misfit dislocations did not add coherently.

Summary

Using high resolution x-ray difractometry , we have examined the fundamental distortions which occur in epitaxial films of lattice-mismatched semiconductors grown on vicinal (100) surfaces miscut from (100) by 2,3, and 4°. We find that there is a non-tetragonal component of the distortion , and that our data indicates a monoclinic unit cell symmetry. Our results agree with predictions calculated by us using the formalism of Hornstra and Bartels[1] which was developed for epitaxial growth on a general (hkl) surface. Lattice tilts were also extracted from our data , and we find that the presence of misfit dislocations did not affect the tilts.

Reference

1. J. Hornstra and W.J. Bartels, J. Cryst. Gowth 44, 513 (1978).
2. D.A.Neumann, H.Zabel, and H. Morkoc, J.Appl. Phys. 64, 3024 (1988).
3. H. Nagai, J. Appl. Phys. 45, 3789 (1974).
4. H.J.Gossmann, B.A.Davidson, G.J.Gualtieri, G.P.Schwartz, A.T.Macrander, S.E. Slusky, M.H.Garbow, and W.A. Sunder, J.Appl. Phys.66,1687 (1989).
5. V. Swaminathan and A.T. Macrander, *Materials Aspects of GaAs and InP Based Structures,* Prentice Hall, NY 1991, Chap. 3.
6. A. Leiberich and J.Levkoff, J. Vac. Sci. Technol. B8,422(1990).
7. E. Anastassakis, Solid State Communications 78, 347 (1991).

END

DATE FILMED

4/23/92